Electrolysis-Bubble-Actuated Micropump

Suyana L. Villarroel
Department of Microelectronic Engineering, 82 Lomb Memorial Dr., Rochester, NY 14623. E-mail: slv8979@rit.edu

Abstract— **An electrolysis-bubble-actuated micro pump is created. The pump is created with a top surface gradient across the channel. This changing gradient will help to propel the bubble, created by electrolysis, forward. This micropump is implemented by taking advantage of both surface tension effect and the electrolysis actuation. The surface tension effect is controlled via the periodic generation of electrolytic bubbles and the roughness gradient design of the microchannel surface. The fabrication of the device was completed following the processes outlined in the design phase. Adhesion problems between the top surface and the silicon substrate were encountered during testing. As result, new layer for better adhesion needs to be implemented in future designs.**

Index Terms—**Bubble, electrolysis, microelectromechanical systems (MEMS) micropump, roughness gradient, surface tension.**

I. Introduction

MICROPUMPS have been the subject of extensive research in both academia and the private sector. In addition, they have been produced in variety of designs that use different actuation mechanisms. Diaphragm micropumps [1] for example, achieve a high volume through a large chamber by using a membrane: however, most techniques for fabricating such diaphragm-based pumps are complicated and involve many photolithographic steps. Another technique [2, 3] drives fluid by applying a high voltage to it. Among such approaches, bubble-actuated valveless micropumps are attractive for their simple operation, miniaturized size, large actuation force, and the ability to physically comply to different types of microchannels with a wide range of cross-sections. Although demonstrated successfully in [4-6], these valveless pumps require a complex time-sequenced power control on many electrodes pairs and a large or long nozzle-diffuser structure. Moreover, further disadvantages include the need for a sealed reservoir inside the fluidic chip.

To overcome the problems presented by other pumps, the top surface of this micropump will have a simple patterned surface with different roughness across in order to propel the bubble that is created forward. This micropump is implemented by taking advantage of both surface tension effect and the electrolysis actuation. The surface tension effect is controlled via the periodic generation of electrolytic bubbles and the roughness gradient design of the microchannel surface.

Compared with other actuation mechanisms, the electrolysis bubble actuator has the features of simple structure, low-power consumption, room temperature operation, and being easy to be integrated into a lab chip. The advantage of this design is the low power consumption and room temperature operation.

II. Device Operation Principle and Microfabrication Process

A. Operation Principle

Figure 1 illustrates the design concept. The device consists of polysilicon electrodes, a hydrophilic microchannel, and a hydrophobic lateral breather connected to air for the elimination of bubbles. The pumping principle—shown schematically from the side in Figure 1(b)—relies on surface tension and multiple bubble-actuation cycles. The actuation mechanism is divided into three phases: bubble generation, degassing, and liquid movement. First, the bubble is generated by electrolysis to push the liquid in whichever direction is required. Next, the bubble is vented out through the lateral breather. At the sides of the microchannel, surface tension exerts a pull on the liquid that creates a characteristic concave shape called a meniscus. Due to the roughness gradient design, the apparent contact angle of the leading meniscus (right) is larger than that of the trailing meniscus (left): $\theta_R > \theta_L > 90°$. Thus, the pressure on the left is larger than that on the right: $P_L > P_R$. As a result, the menisci respond with different velocities, and a net pumping flow along the x direction is achieved. Displacement of the liquid occurs through repetition of these cycles.

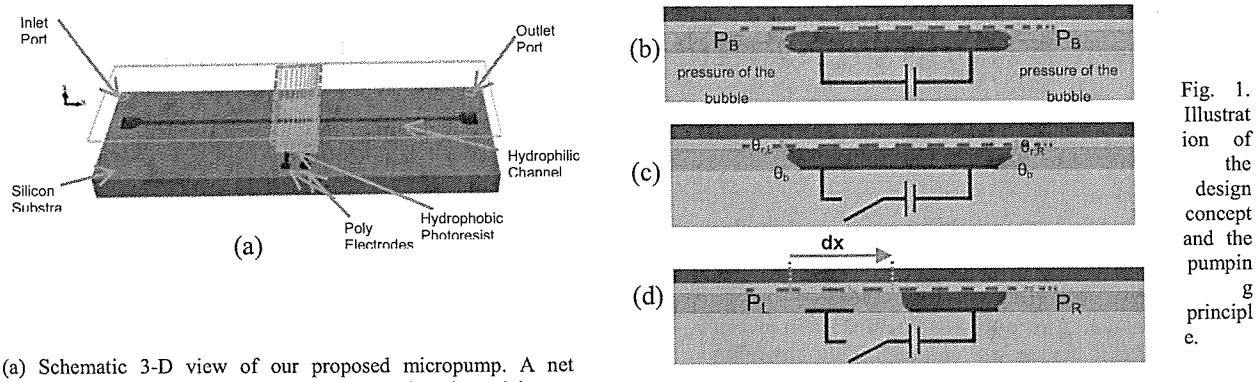

Fig. 1. Illustration of the design concept and the pumping principle.

(a) Schematic 3-D view of our proposed micropump. A net pumping flow along the x-direction of the microchannel in one pumping cycle via three processes [(b) bubble generation, (c) degassing, and (d) liquid movement] is illustrated from the side views of the micropump. The net pumping fluid is achieved over multiple electrolysis bubble actuation cycles in the microchannel. Here, P_b, P_L,and P_R are the pressures. $\theta_{r,L}$, $\theta_{r,R}$,and θ_b are the contact angles.

The net volume displacement of liquid and the pumping rate are dominated by the geometry design of the microchannel, the design of the roughness gradient surface, the frequency and amplitude of the applied voltage, and the design of the electrodes. All details will be described with the experimental results later in this paper.

B. Microfabrication

The microfabrication process for our micropump is illustrated in Fig. 1(a).First, a standard n-type 100 silicon substrate is grown with the thermal oxide of 500Å. Then 1500Å of Silicon nitride are deposit. These are lithographically patterned with the channel. Then, the substrate is etched by the wet etching process in KOH solution to define the microchannel. A BOE etch of one minute is perform to remove the 500Å of oxide. Then the substrate is grown with another 6500Å thermal oxide. This thermal oxide is only deposit in the channel surface to form the hydrophilic layer. The Silicon nitride is then removed so the silicon substrate is the exposed. Poly silicon is deposit, 6000Å for the formation of the electrodes. Next, Positive photoresist is spin coated on the wafer and cured at in a high-temperature oven. The photoresist is lithographically patterned and etched as hydrophobic regions by the O2 plasma process to serve as the bottom part of the hydrophobic lateral breather. The top cover with the roughness gradient structure is fabricated by using a dry film negative photoresist. A first layer is exposed first and then a second layer with the pattern is mounted.

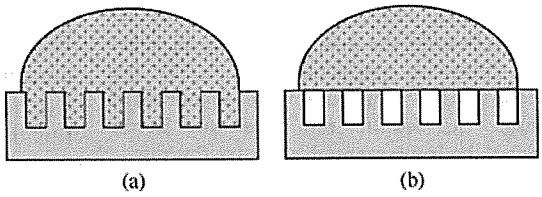

Fig. 2. Droplet on the surface forms: (a) the complete wetting and (b) the composite wetting based on the hydrophilic and the hydrophobic properties of substrate surfaces, respectively.

III. Theoretical Analysis

A. Roughness Gradient Design of Hydrophobic Surface

The contact angle has been commonly used to represent surface wettability. Surface wettability is a function of surface roughness. The latest experimental results confirm that wettability can be tuned by surface roughness [25], [26]. The earliest literatures reported that the contact angle of a droplet on a rough surface could be predicted by two main theories relating the surface structure to the apparent contact angle. The first theory was proposed by Wenzel [27], which assumes that the liquid completely wets the solid structure, as illustrated in Fig. 2(a). The second theory was proposed by Cassie and Baxter [28], which assumes that the liquid does not wet the valleys of the structure and forms a composite surface on the rough substrate, as illustrated in Fig. 2(b). Afterwards, Bico *et al.* [26] fabricated the substrates with specific roughness and compared the measured contact angles with the prediction results. They claimed good agreement and proposed that Wenzel's formula is valid for the hydrophilic surface and that Cassie and Baxter's formula is valid for the hydrophobic surface.

The structural design of the surface roughness gradient in our device is illustrated in Figure 3. The surface roughness varies with the pillar patterns on the dry film resist cover. For our roughness gradient design, pillar decreases along the x-direction of the microchannel.

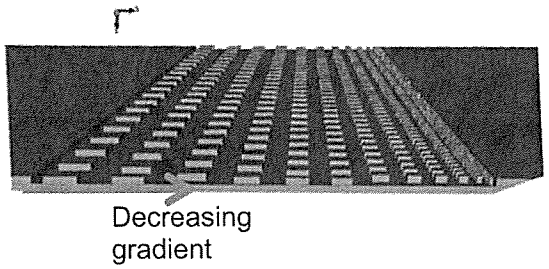

Fig. 3. Illustration of the roughness gradient design on the hydrophobic surface of the top dry film resist cover that is made of square pillars

The roughness gradient surface of our micropump is hydrophobic, which leads to the formation of a composite surface. Besides, previous report from Shirtcliffe *et al.* has also shown that the dimension variation of square pillars allows the length of the contact perimeter per unit area to be varied without varying the contact area per unit area [30]. As a result, there is no change on the contact angles.

B. Electrolysis

When an electric current is sent through the two noble metal electrodes (such as platinum) in water, electrolysis takes place. The minimum equilibrium potential of hydrogen–oxygen electrolysis E^{0} is 1.23 V. In the electrolysis reaction, the oxygen gas is produced at the anode, and the hydrogen gas is produced at the cathode, i.e.

$$anode: 2H_2O \rightarrow 4H^{+}4e^{-} + O_2$$

$$cathode: 2H_2O + 2e^{-} \rightarrow 2OH^{-} + H_2$$

Under the assumption that all generated gases (O_2 and H_2) evolve in the form of gas bubbles, the total gas volume linearly depends on the input electrical charge [17]. The total gas volume generated by the electrolysis in the process of bubble nucleation could be estimated according to Faraday's law of electrolysis and the ideal gas law [31]

$$N = \frac{It}{zF}$$

$$PV = NRT$$

where N is the moles of produced gas, I is the applied current, z is the number of excess electrons, F is Faraday's constant (9.649×10^{4} C/mol), t is the period of electrolysis, T is temperature, P is the ambient pressure, V is the volume of the bubble, and R is the gas constant (8.314 J K^{-1}/mol). Under the assumption of constant temperature and atmospheric pressure, the volume of produced gases is proportional to the supplied electric current [32].

D. Applied Voltage

The pumping flow rate relies on many factors, such as the applied voltage, the duty cycle, and the driving frequency. These imply that the actuation pulses play a dominant role for the maximum pumping flow rate. Besides, the expansion period and the venting period of the bubble in one pumping cycle are also critical parameters to regulate the square-wave actuation pulses. The operation frequency f and the duty ratio d are defined as

$$f = \frac{1}{t_{expand} + t_{vent}} \quad (1)$$

$$d = \frac{t_{expand}}{t_{expand} + t_{vent}}$$

where t_{expand} and t_{vent} are the expansion period and the venting period of the electrolytic bubble in one pumping cycle. The expansion period t_{expand} is dominated by the period of the applied voltage in one pumping cycle. The venting period t_{vent} is dominated by the bubble volume and the pressure magnitudes on both meniscuses.

IV. Experimental Setup

To characterize the performance of the micropump with different depths were fabricated. The test was done by using low-power oscillators to create the square waveforms required by each poly-electro to generate the bubble.

V. Experimental Results and Discussion

Fig. 6(a) shows a prototype device made of the dry film resist. The fabrication of the device was completed following the processes outlined in the design phase, but adhesion problems between the top layer and the silicon substrate were encountered during testing. This problem made it impossible to acquire data for the characterization of the micropump.

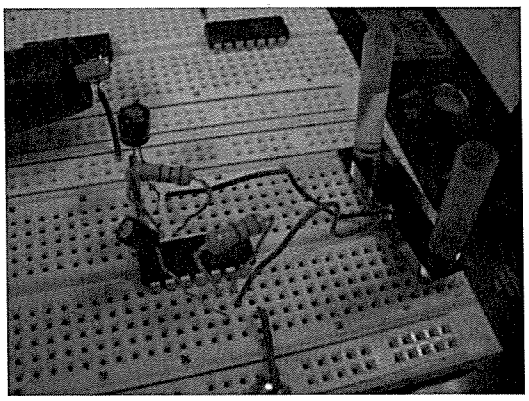

Fig. 6. Experimental setup of device with a micropump with a depth of 100μm.

VI. Conclusion

A electrolysis-bubble-actuated micropump with the design of the roughness gradient on the microchannel hydrophobic surface and the lateral breather was successfully fabricated. Further work to optimize the adhesion between the dry film resist and the silicon surface is need. The features of micropumps on compact size, simple microfabrication, low-power consumption, and room temperature operation make it promising to be integrated with other multiple components to form microfluidic systems.

References

[1] H. Andersson, *et al,* "A valve-less diffuser micropump for microfluidic analytical systems", *Sensors and Actuators B: Chemical* Volume 72, Issue 3, Pages 259-265, 2001

[2] D. Stroock, *et al,* "Patterning electro-osmotic flow with patterned surface charge", *Physics Review Letters,* vol. # 84 (15), pp. 3314–3317, 2000.

[3] A. Richter, *et al,* "A micromachined electrohydrodynamic (EHD) pump, *Sensors and Actuators,* vol. A 29 (2), pp. 159–168, 1991.

[4] T. K. Jun , *et al,* "Valveless pumping using traversing vapor bubbles in microchannels", *Journal of Applied Physics,* vol. 83 (11), pp. 5658–5664, 1998.

[5] J. H. Tsai, *et al,* "A thermal-bubble-actuated micronozzle-diffuser pump", *Journal of Microelectromechanical Systems,* vol. 11 (6), pp. 665–671, 2002.

[6] S. Bohm, *et al,* "A closed-loop controlled electrochemically actuated micro-dosing system", *Journal of Micromechanical Microenginering.* Vol. 10, pp. 498–504, 2000.

[7] S. Böhm, B. Timmer, W. Olthuis, and P. Bergveld, "A closed-loop controlled electrochemically actuated micro-dosing system," *J. Micromech. Microeng.*, vol. 10, no. 4, pp. 498–504, 2000.

[8] S. Shibuichi, T. Onda, N. Satoh, and K. Tsujii, "Super water-repellent surfaces resulting from fractal structure," *J. Phys. Chem.*, vol. 100, no. 50, pp. 19 512–19 517, 1996.

[9] J. Bico, C. Marzolin, and D. Quéré, "Pearl drops," *Europhys. Lett.*, vol. 47, no. 2, pp. 220–226, 1999.

[10] R. N. Wenzel, "Surface roughness and contact angle," *J. Phys. Colloid Chem.*, vol. 53, no. 9, pp. 1466–1467, 1949.

[11] A. Shastry, M. J. Case, and K. F. Böhringer, "Directing droplets using micro-structured surfaces," *Langmuir*, vol. 22, no. 14, pp. 6161–6167, Jul. 2006.

[12] N. J. Shirtcliffe, S. Aqil, C. Evans, G. McHale, M. I. Newton, C. C. Perry, and P. Roach, "The use of high aspect ratio photoresist (SU-8) for super-hydrophobic pattern prototyping," *J. Micromech. Microeng.*, vol. 14, no. 10, pp. 1384–1389, Oct. 2004.

[13] S. Böhm, W. Olthuis, and P. Bergveld, "An integrated micromachined electrochemical pump and dosing system," *J. Biomed. Microdev.*,vol.1, no. 2, pp. 121–130, Dec. 1999.